Optimizing Interface Conductivity in Electronics

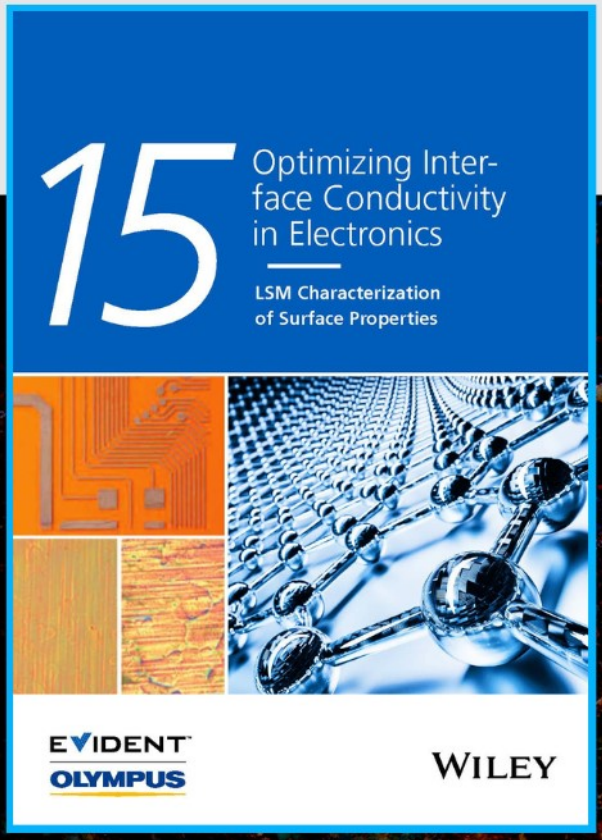

The latest eBook from Advanced Optical Metrology. Download for free.

Surface roughness is a key parameter for judging the performance of a given material's surface quality for its electronic application. A powerful tool to measure surface roughness is 3D laser scanning confocal microscopy (LSM), which will allow you to assess roughness and compare production and finishing methods, and improve these methods based on mathematical models.

Focus on creating high-conductivity electronic devices with minimal power loss using laser scanning microscopy is an effective tool to discern a variety of roughness parameters.

EVIDENT
OLYMPUS

WILEY

ADVANCED ELECTRONIC MATERIALS Open Access
www.advelectronicmat.de

Ultralow Thermal Conductivity Achieved by All Carbon Nanocomposites for Thermoelectric Applications

Saqib Rafique, Matthew R. Burton, Nafiseh Badieh, Shahin Mehraban, Afshin Tarat,* Guangzheng Zuo, Lijie Li,* and Yiqiang Zhan**

Carbon-based materials are becoming a promising candidate for thermoelectricity. Among them, graphene shows limited scope due to its ultra-high thermal conductivity (κ). To develop graphene-based thermoelectric devices, reduction of κ is highly desired while maintaining reasonably high electrical conductivity (σ). Herein, multiwalled carbon nanotubes (MWCNTs) and carbon black (CB) fillers are added into few layered graphene (FLG) to produce all-carbon composites yielding ultra-low thermal conductivity (κ) desired for thermoelectric applications. The novel preparation method of pristine FLG realizes very low κ of 6.90 W m^{-1} K^{-1} at 1248 K, which further reduces to 0.57, 0.81, and 0.69 W m^{-1} K^{-1} at the same temperature for FLG + MWCNTs, FLG + CB, and FLG + MWCNTs + CB, respectively. As-prepared FLG composites also maintain reasonably high σ, whilst the Seebeck coefficient shows over a factor of five improvement after the inclusion of carbon-based fillers. Consequently, the power factor (PF) is significantly improved. The ultralow κ is attributed to the increased thermal boundary resistance among graphene sheet boundaries. The realization of ultralow κ with simultaneous improvement in Seebeck coefficients and relatively small drops in σ with a facile and unique synthesis technique, highlight the potential of these composites.

1. Introduction

Due to the effects of climate change and the dwindling supply of fossil fuels, a transition to sustainable energy sources is required. In the UK alone, 48 TW h^{-1} yr^{-1} of energy is lost through industrial waste heat.[1] Thermoelectric (TE) materials prepared from cost-effective and abundant elements have gained remarkable attention for sustainable waste heat recovery due to almost all commercial TE materials containing Earth rare elements.[2,3] The conversion efficiency of TE materials is determined by the dimensionless figure of merit ZT = S2$\sigma T/\kappa$, where S, σ, T, and κ represent the Seebeck coefficient (V K^{-1}), electrical conductivity (S m^{-1}), absolute temperature (K), and thermal conductivity (W m^{-1} K^{-1}), respectively.[4] A higher ZT can be achieved by improving the power factor (PF = S2σ) and simultaneously reducing the κ.[5] These parameters; however, are interrelated through the carrier concentration, and a distinctive control on either of PF or κ is a real challenge. Several strategies have been reported to enhance the ZT such as carrier concentration modulation through resonant energy doping,[6] band engineering,[7] and energy filtering of carriers[8] for higher PF while the κ can be reduced by introducing point defect,[9,10] dislocations,[11,12] grain boundaries,[13] and incorporation of nanomaterials.[14]

S. Rafique, G. Zuo, Y. Zhan
Center for Micro Nano Systems
School of Information Science and Technology (SIST)
Fudan University
200433 Shanghai, P. R. China
E-mail: yqzhan@fudan.edu.cn

M. R. Burton
SPECIFIC-IKC
Department of Materials Science and Engineering
Faculty of Science and Engineering
Swansea University
SA1 8EN Swansea, UK
E-mail: m.r.burton@swansea.ac.uk

The ORCID identification number(s) for the author(s) of this article can be found under https://doi.org/10.1002/aelm.202300023

DOI: 10.1002/aelm.202300023

N. Badieh, L. Li
College of Engineering
Swansea University
SA1 8EN Swansea, UK
E-mail: l.li@swansea.ac.uk

S. Mehraban
MACH 1
Faculty of Science and Engineering
Swansea University
SA1 8EN, Bay Campus Swansea, UK

A. Tarat
C6 Tech
Unit 3 Oxwich Court
SA6 8RA, Valley way, Enterprise Park Swansea, UK
E-mail: afshin.tarat@swansea.ac.uk

The current state-of-the-art TE technology is largely reliant on inorganic solid state materials which exhibit high ZT values, such as SnSe,[15,16] PbTe,[17,18] and Bi2Te3.[19] They are; however, mechanically rigid, brittle, expensive, naturally scarce toxic materials, which limit their widespread applications and therefore raise the interest in abundant, nontoxic, inexpensive, and mechanically resilient organic materials for thermoelectric applications.[20,21] In recent years, organic TE materials have made profound progress and their figure of merit is approaching to the inorganic TE materials owing to the optimization of their morphology (molecular) design,[22] distinctive transport pathways, and device geometries[21] as well as doping or inclusion of organic/inorganic TE materials.[23,24] In this context, low-dimensional carbon-based TE materials are promising candidates for thermoelectricity.[25–28] Particularly, graphene (a monolayer of sp2-hybridized carbon atoms) is a promising 2D material because of its unique properties such as: non-toxicity, tuneable properties, large-scale synthesis routes, thermal stability, and exceptionally high intrinsic carrier mobility (μ) in electrical transport and flexibility.[28,29] Graphene; however, as a TE material has shown limited scope due its significantly high in-plane thermal conductivity, and its semi-metallic characteristics yield limited Seebeck coefficient,[30,31] which lead to a modest thermoelectric conversion efficiency determined by the ZT.[27] TE properties of graphene; however, can be modified via doping, nano-inclusion, and structural defects.[32] It is highly desired to reduce thermal conductivity while maintaining a reasonable electrical conductivity. Thermal conductivity can be viewed as the product of the electrical and lattice components. Whilst the electrical component of thermal conductivity (κe) is strongly coupled with electrical conductivity through the carrier concentration, the lattice component of thermal conductivity (κL) is independent of carrier concentration.

In an effort to improve TE conversion efficiency of graphene, we recently demonstrated high quality, defect free few layered graphene (FLG) prepared via a novel dry physical grinding method.[33] The resultant, FLG, showed significantly lowered thermal conductivity (6.90–10.77 W m^{-1} K^{-1} between 323 and 1274 K) parallel to pressing direction compared to FLG values reported in the literature, which was anticipated to further reduce via doping or nanoinclusion. In this context, the current work, demonstrates ultra-low thermal conductivity of FLG composite with 5 wt% of multi-walled carbon nanotubes (MWCNTs), carbon black (CB), and a composite of both, which are mixed using blender (VEVOR Electric Grain Mill 1800 W) and named hereafter FLG + MWCNTs, FLG + CB, and FLG + MWCNTs + CB, respectively. The resultant composites show exceptionally lower thermal conductivity of between 0.3 and 0.98 W m^{-1} K^{-1} in the temperature range between 323–1274 K, when compared to pristine FLG. To the best of our knowledge, these are amongst the lowest thermal conductivity values for FLGs reported so far; while, the electrical conductivity only reduced to around factor of 2.5. Moreover, Seebeck coefficient has also seen a pronounced increase resulting in a significant increase in the power factor of the composite FLG.

2. Results and Discussion

Figure 1 shows schematic of the current work, Figure 1a illustrates the pellet making process, while Figure 1b shows the CB

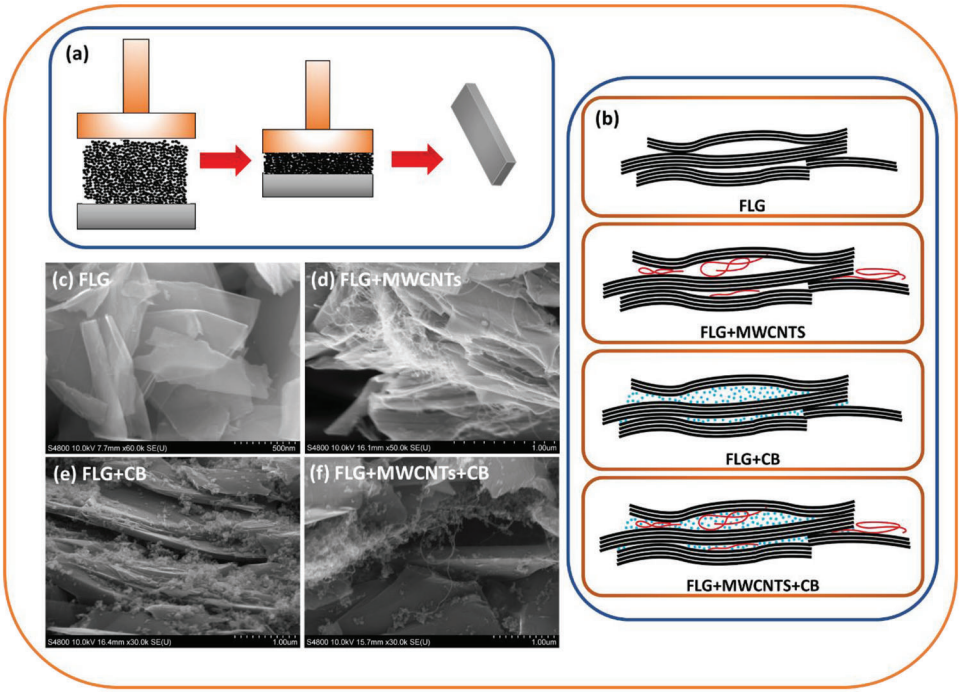

Figure 1. Schematic illustration of the current work. a) Schematic of pellet making process. b) Schematic showing existence of carbon-based fillers between the sheets of FLGs, and corresponding c–f) SEM images showing the same. SEM images of Pure FLG (c), FLG + MWCNTs (d), FLG + CB (e), and FLG + MWCNTs + CB (f).

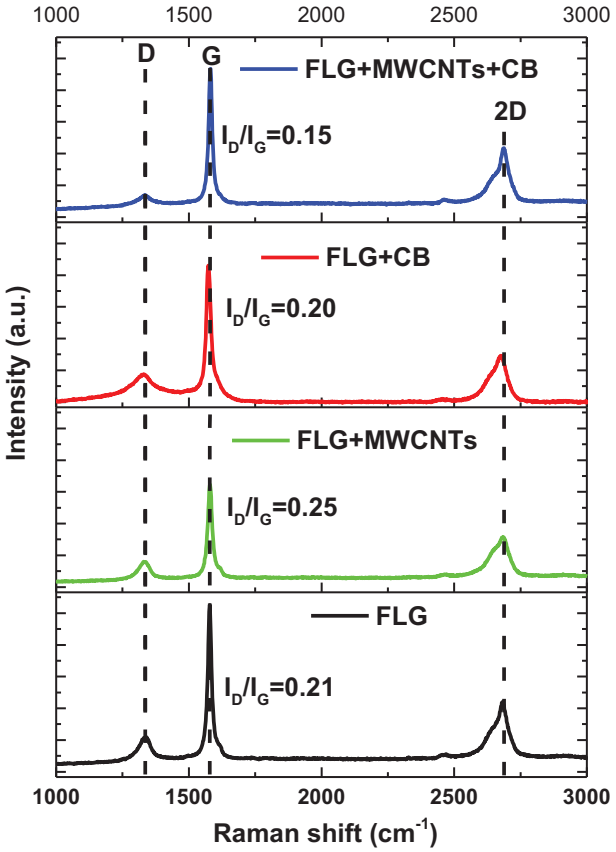

Figure 2. Raman spectra of pristine FLG, FLG + MWCNTs, FLG + CB, and FLG + MWCNTs + CB.

and MWCNTs-based fillers which are settled into the spaces between the FLG sheets. In addition, the corresponding SEM images (c–f) also show the existence of these CB and MWCNTs-based fillers into the spaces between the FLG sheets. Pristine FLG (Figure 1c) clearly shows ultra-thin and stacked few layers of graphene sheets, while the inter-sheet spacing can also be seen, indicating high level of exfoliation. The SEM images of FLG + CB (Figure 1d), FLG + MWCNTs (Figure 1e), and FLG + MWCNTs + CB (Figure 1f) show that these carbon-based additives are inserted into the inter-layer space of FLG, creating additional boundaries between the FLG layers. Moreover, the inclusion of these additives ultimately is likely to have pushed the layers further apart, as can be seen in the SEM images for composites.

The effect of all-carbon additives modification of FLG load matrix has been further elucidated by Raman spectroscopy. Raman spectroscopy of the pristine FLG and its carbon-based composites is shown in **Figure 2**. All the representative spectra show singular D and G peaks with the low I_D/I_G ratio for FLG (0.21) as well as its CNT (0.25) and CB (0.20) or both (0.15) based variants; the variation in the peak ratio can be attributed to random variation in FLG thicknesses and defects at the particular sites investigated rather than any effect caused by the MWCNTs and CB. The low I_D/I_G ratios indicate that FLG has not been considerably affected by the addition of carbon-based fillers.[27] Moreover, it also indicates the crystallinity of the samples did not significantly alter.[34] It is observed that the peak position of D-band (≈1340 cm^{-1}), G-band (≈ 1580 cm^{-1}), and 2D-band (2685 cm^{-1}) did not show an obvious shift, which implies that addition of CNT or CB did not cause the softening or hardening of phonons.[35] The lower I_D/I_G ratio of our samples as compared to reported data for FLGs[27] and the least defects as indicated by very low peak intensity of D-band demonstrate the high quality of the prepared material and fewer layers of the prepared FLG.[33] It is noteworthy that low intensity peak of the D-band indicates the lesser defects in the honeycomb structure because D-band represents the structural defects in the graphene which are ascribed to the imperfections in the discrete hexagons in the honeycomb structure of graphene.[36] Moreover, the I_D/I_G ratio is directly proportional to the number of layers in FLG.[37]

Figure 3a shows the electrical condutivity perpendicular to the pressing diretion of FLG and its carbon based composite variants as a function of temperature (316–895 K). Pristine FLG and the composite variants show similar trends in electrical conductivity, with a positive linear corrolation with temperature, indicating that all samples exhibit semiconducting behavior. The addition of MWCNTs, CB, or both is shown to lower the electrical condutivity of the resultant composites. MWCNTs are seen to have the most pronounced effect, dropping the electrical conductivity by around a factor of ≈2.5 throughout all temperatures studied, whilst CB and MWCNTs plus CB both have electrical conductivities between pristine FLG and MWCNTs fillers based FLG. A sizeable increase of the Seebeck coefficient is observed upon all carbon-based fillers variants. All Seebeck coefficients are observed to be positive, indicating that the p-type character of the materials is preserved. The highest recorded Seebeck coefficient observed is for the FLG + MWCNTs composite, 25.4 μV K^{-1} at 374 K. This is significantly higher than FLG at the same temperature (1.5 μV K^{-1}) and higher than the highest value observed for pristine FLG (3.9 μV K^{-1} at 895 K). FLG + CB and FLG + MWCNTs + CB composites follow the same Seebeck temperature trend as FLG + MWCNTs, albeit with slightly diminished values. The highest recorded values are 22.3 μV K^{-1} and 20.4 μV K^{-1} at 374 K, for FLG + CB and FLG + MWCNTs + CB, respectively. The simulations decrease in electrical conductivity and increase in the Seebeck coefficient of all the carbon-fillers based semiconducting FLG samples indicates a reduction in the carrier concentration is caused via all additives are used. The Seebeck coefficients (Figure 3b) decline with an increase in temperature, with some regions seeing a more pronounced decrease than others. FLG, however, exhibits a semi-linear increasing trend in Seebeck coefficient, reaching 3.9 μV K^{-1} at 895 K, which is believed to be due to a small change in the electrochemical potential and a large degree of hole hopping.[33] The power factor values for FLG remain below 1 μW m^{-1} K^2 over the entire temperature range between 315 and 895 K. The inclusion of MWCNTs and/or CB; however, due to the substantially increased Seebeck coefficients, increases the power factor up to a maximum value of 15.3 μW m^{-1} K^{-2} for the FLG + CB and 13.2 μW m^{-1} K^{-2} for the FLG + MWCNTs composite over the same temperature range. The FLG + MWCNTs+CB ternary composite also shows similar trend and power factor values reach up to 14.7 μW m^{-1} K^{-2}. Among these composites, the power factor values for FLG + MWCNTs remain stable over the entire temperature range as shown in Figure 3c. The power factor plots predominantly follow the same trend as that of Seebeck coefficients due to the very linear nature of the

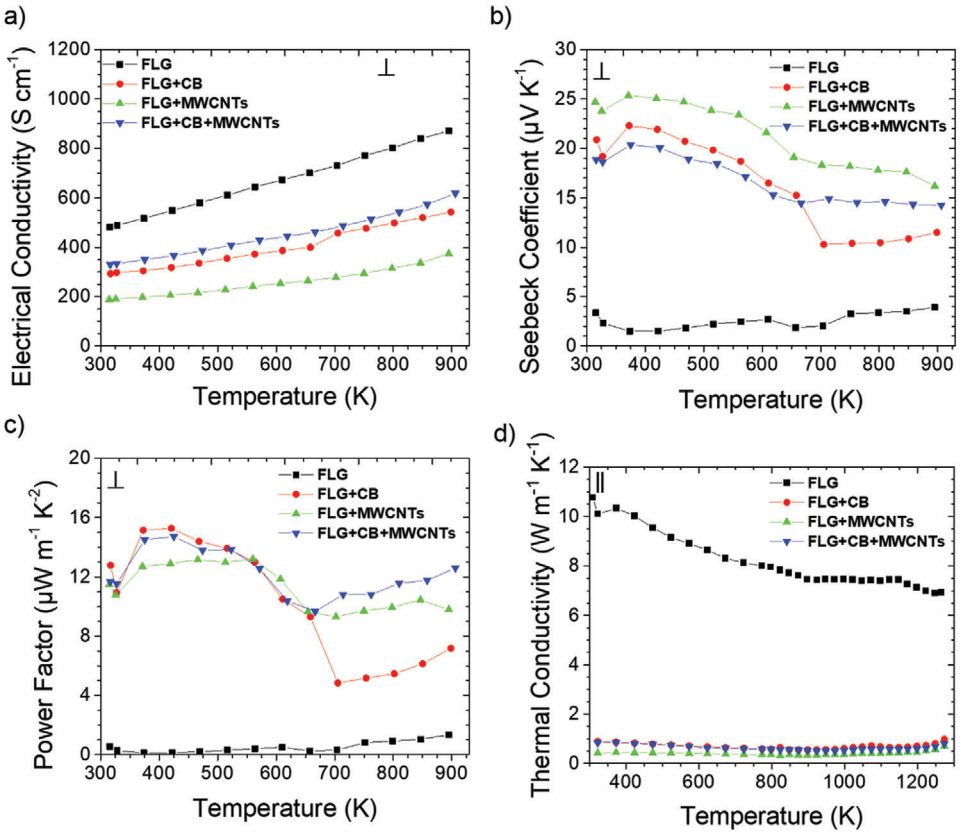

Figure 3. Thermoelectric characterization. a) Electrical conductivity, b) Seebeck coefficient, c) power factor, and d) thermal conductivity of pristine FLG plus its FLG + MWCNTs, FLG + CB, and FLG + MWCNTs + CB based all-carbon composites. Data for pristine FLG has been obtained from our previous work. Reproduced with permission.[33] Copyright 2020, American Chemical Society.

electrical conductivities and power factors dependence on the square of Seebeck. All samples are run through a second thermal cycle (Figure S2, Supporting Information), whilst there is a marginal drop in electrical conductivity and a marginal increase in Seebeck coefficients seen across all samples; within measurement uncertainty, the values are the same. This indicates that the samples are thermally stable.

The strongest change in thermoelectric properties is seen in thermal condutivity, measured parellel to the pressing direction (thermal diffusivity and heat capacity can be seen in Figure S1, Supporting Information). An unprecidented drop for the composite variants of FLG was observed, up to a factor of 20 reduction for FLG + MWCNTs, as shown in Figure 3d. Almost similar falling trends were observed for the FLG + CB and FLG + MWCNTs + CB composites. To the best of our knowledge, the thermal conductivity of FLG after inclusion of MWCNTs and/or CB is one of the lowest ever reported values for graphene. **Table 1** compares the thermal conductivity values of FLG reported in literature with the thermal conductivity values of the present work for the pristine FLG and its carbon-based composites. The lowest thermal conductivity was observed for the FLG + MWCNTs composite (0.32–0.70 W m^{-1} K^{-1} at 323–1273 K), which is consistent with the least electrically conductive sample because both the thermal and electrical conductivities are strongly coupled with each other via the carrier concentration. The thermal conductivity (κ) of TE materials can be summarized as the product of two components; 1) electronic component (κ_e), where electrons and holes transport heat and 2) lattice component (κ_l), where phonons travel through the lattice ($\kappa = \kappa_e + \kappa_l$). An ideal TE material requires a charge carrier concentration of a heavily doped semiconductor and a small lattice thermal conductivity to yield high ZT.[38,39] The electrical component of thermal conductivity is directly related to the electrical conductivity through the Wiedemann–Franz law ($\kappa_e = L.\sigma.T$).[39] The substantial drop in the thermal conductivity of the MWCNTs and CB based FLG composites therefore cannot be explained by its electrical component alone. This decrease can be explained due to the existence of CB and MWCNTs between graphene layers as evidenced by the SEM images (Figure 1). The addition of CB/MWCNTs between graphene layers likely has the result of introducing a significant increase in thermal boundary resistances, reducing the lattice thermal conductivity. Existence of MWCNTs and CB between the FLGs also would have resulted in slight increases in the gaps between the FLGs, leading to increased phonon scattering; and thus, reduction in the lattice component of thermal conductivity.[33] Additive particles are not more than 5% of the samples; therefore, electrical conductivity should only be slightly to moderately decreased depending on the number of disconnections between graphene sheets. Making pellet from nano sheets ultimately results in some gaps between the sheets, resulting in affecting the thermal conductivity of the

Table 1. Comparison of the thermal conductivity values of the graphene reported in the literature and the present work.

Material	Thermal conductivity values [Wm^{-1} K^{-1}]	T [K]	Plane-orientation	Ref.
Graphene	≈4000	≈320	In-plane	[40]
Suspended single layered graphene (SLG)	≈4840–5300	RT	–	[41]
Suspended graphene	≈3000–5300	RT	In-plane	[42]
Pyrolytic graphite	≈2000	RT	In-plane	–
Pure pitch-bonded graphite	≈200	RT	In-plane	[43]
FLG (n = 2–4)	≈2800–1300	RT	In-plane	[44]
SLG	600	RT	–	[45]
Suspended graphene	≈2600–3100	350	In-plane	[43]
Porous 3D-graphene networks	0.54–0.90	298–773	–	[34]
Graphene nanoribbon(n < 5)	≈1000–1400	RT	–	[46]
Oxygen plasma treated defected graphene supported on substrate	36	–	–	[47]
Graphene pellet	0.38–3.02	303–363	Parallel to the pressing direction	[48]
MWCNT pellet	1.60–2.25	300–923	Parallel to the pressing direction	[49]
Carbon black pellet	≈0.2–0.4	350–475	Parallel to the pressing direction	[50]
Pristine FLG	6.91-10.77	323–1273	Parallel to the pressing direction	Present work
FLG + MWCNTs	0.32–0.70	323–1273	Parallel to the pressing direction	Present work
FLG + CB	0.55–0.98	323–1273	Parallel to the pressing direction	Present work
FLG + MWCNTs + CB	0.50–0.80	323–1273	Parallel to the pressing direction	Present work

pellet which is predictably lower than the graphene sheets. Whilst a true ZT could not be determined because the power factor and thermal conductivity were measured along different planes relative to the pressing direction, if the thermal conductivity was subdued by the same factor against the pressing direction, a ZT of 0.002 (Figure S3, Supporting Information) would be seen for MWCNTs fillers based FLG at 895 K, an improvement by over a factor of 160 compared to FLG, with improvements near 1000× seen at other temperatures. It must be stressed; however, that this is just a hypothesized ZT as thermal conductivity was measured along a different plane to the other properties.

Our composites are shown to have lower thermal conductivity than pristine FLG and a comparable pellet of graphene or MWCNT measured along the same plane,[48,49] with a carbon black pellet exhibiting similar levels of thermal conductivity.[50] Single layer graphene exhibits very high thermal conductivity;[51] however, several theoretical (molecular and lattice dynamics simulations) studies reveal that the addition of a few layers can significantly reduce the thermal conductivity.[52] This has been exactly demonstrated by the pristine FLG sample which shows significantly lower thermal conductivity as compared to the reported values.[44] It is noteworthy that inter-layer spacing also play a substantial role in further reducing the thermal conductivity. Moreover, inclusion of carbon-based additives, particularly, between the graphene layers can be an effective strategy to lower the thermal conductivity of the graphene while maintaining the reasonably high electrical conductivity, as it can be seen in the current study. The additives have moved into the inter-layer spacing and notably reduced the connections between the FLGs.[35] Moreover, heterogenous interfacial sites have been formed due to loading of MWCNTs and CB additives onto the graphene surface; this phenomenon may lead to an extremely high phonon-scattering; and thus, renders exceptionally lower thermal conductivities owing to limited thermal transport and an increased thermal resistance.[35,52]

3. Conclusion

In summary, an all-carbon based thermoelectric materials concepts has been developed with a simultaneous improvement in the power factor and reduction in thermal conductivity. Ultralow thermal conductivity of FLG has been realized by introducing 5% MWCNTs and/or CB into the FLG matrix. The samples were prepared using a novel dry physical grinding technique followed by blender mixing. The resultant MWCNTs and CB-based FLG composite exhibited ultralow thermal conductivity typically below 1 W m^{-1} K^{-1}, which is amongst the lowest reported thermal conductivity values of FLG based all-carbon composites. The composites also showed more than five-times improvement in the peak Seebeck coefficient values: from 3.9 μV K^{-1} at 895 K for pristine FLG to 25.4, 22.3, and 20.4 μV K^{-1} at 374 K for FLG + MWCNTs, FLG + CB, and FLG + MWCNTs + CB, respectively.

Consequently, the power factor has been improved from 1.3 μW m^{-1} K^{-2} at 895 K for pristine FLG to a maximum value of 15.3 μW m^{-1} K^{-2} at 422 K for FLG + CB, 13.2 μW m^{-1} K^{-2} at 563 K for FLG + MWCNTs, and 14.7 μW m^{-1} K^{-2} at 422K for FLG + MWCNTs + CB composites. While the composites did show a reduction in the electrical conductivity by around a factor of 3, this was insignificant when compared to the reduction in the thermal conductivity which has been reduced by more than a factor of 20. This significant reduction in thermal conductivity is attributed to the settling of MWCNTs and/or CB additives between the inter-layer spacing (as shown by SEM), leading to reduced interactions between the FLGs and high phonon scattering probability due to increased thermal boundary resistance. The challenge is now to further optimize the Seebeck coefficient to achieve ZT over 1 while maintaining the ultralow thermal conductivity of the FLG-based all carbon composites. One potential route to this is introducing a small amount of inorganic TE materials into the FLG matrix.

4. Experimental Section

Materials Preparation: FLG was prepared following the authors' previously reported synthesis route.[33] MWCNTs (NANOCYL NC7000 series) were obtained from Nanocyl SA, Belgium, and the CB was obtained from Imerys S.A., France. First, the FLG powder was transferred into the stainless-steel mold under 10 tons cm^{-2} for 2 min to prepare pure FLG samples. Further, 5 wt% MWCNTs were added to 95 wt% of FLG powder using blender (VEVOR Electric Grain Mill (1800 W) for 10 min to achieve the highest level of uniformity possible; then, the mixture was transferred into the stainless-steel (304 grade) mold under 10 tons cm^{-2} for 2 min to prepare pure FLG + MWCNTs samples. This pressure was chosen as pressures under 5 tons resulted in fragile and spongy structures, and at pressures over 10 tons, the molds started to be deformed and damaged. In addition, no difference between the as-fabricated graphene pellets over 10 tons was observed. Similarly, 5 wt% CB was blended with 95 wt% FLG, and stainless-steel mold was used under 10 tons cm^{-2} for 2 min to prepare FLG + CB samples. For the ternary composite, 2.5 wt% CB and 2.5 wt% MWCNTs were added to 95 wt% FLG powder using blender (VEVOR Electric Grain Mill 1800 W); then, the mixture was transferred into the stainless-steel mold under 10 tons cm^{-2} for 2 min to prepare pure FLG + MWCNTs + CB samples.

Characterizations: Morphology of the FLG and its composites has been characterized by field emission scanning electron microscope, (FE-SEM, Hitachi 4800 S, Japan). Thermoelectric characterization: electrical conductivity and Seebeck coefficients were determined with an ULVAC ZEM-3 with a helium atmosphere, while thermal conductivity ($\kappa = DC_p\rho$) was determined by measuring the thermal diffusivity (D) and heat capacity (C_p) with a Netzsch LFA 457 (Figure S1, Supporting Information); whilst densities (ρ) were determined using the method of hydrostatic weighing that uses the Archimedes principle (Table S1, Supporting Information).

Supporting Information

Supporting Information is available from the Wiley Online Library or from the author.

Acknowledgements

S.R. and M.R.B contributed equally to this work. This work was supported by the National Natural Science Foundation of China under the grant number 62274040. M.R.B. would like to acknowledge EPSRC (EP/N020863/1) and the European Regional Development Fund (c80892) through the Welsh Government for funding. M.R.B. would also like to thank EPSRC (EP/S018107/1). S.M. wishes to thank the Welsh Government, ERDF, and SMARTExpertise Wales for funding MACH1 and COMET. The affiliation details for L.L. were altered after initial online publication in July, 2023.

Conflict of Interest

The authors declare no conflict of interest.

Data Availability Statement

The data that support the findings of this study are openly available in [NAME] at [DOI], reference number [REF].

Keywords

all-carbon, few layered graphene, thermoelectrics, ultra-low thermal conductivity

Received: January 12, 2023
Revised: April 5, 2023
Published online: May 5, 2023

[1] J. Besseling, H. Pershad, *The Potential for Recovering and Using Surplus Heat from Industry Final Report*, London, **2014**.
[2] M. S. Dresselhaus, G. Chen, M. Y. Tang, R. G. Yang, H. Lee, D. Z. Wang, Z. F. Ren, J.-P. Fleurial, P. Gogna, *Adv. Mater.* **2007**, *19*, 1043.
[3] H. Jeong, S. K. Kihoi, H. Kim, H. S. Lee, *J. Mater. Res. Technol.* **2021**, *15*, 6312.
[4] A. Zevalkink, D. M. Smiadak, J. L. Blackburn, A. J. Ferguson, M. L. Chabinyc, O. Delaire, J. Wang, K. Kovnir, J. Martin, L. T. Schelhas, T. D. Sparks, S. D. Kang, M. T. Dylla, G. J. Snyder, B. R. Ortiz, E. S. Toberer, *Appl. Phys. Rev.* **2018**, *5*, 021303.
[5] A. Mehdizadeh Dehkordi, M. Zebarjadi, J. He, T. M. Tritt, *Mater. Sci. Eng., R* **2015**, *97*, 1.
[6] M. Hong, Z. G. Chen, L. Yang, Y. C. Zou, M. S. Dargusch, H. Wang, J. Zou, *Adv. Mater.* **2018**, *30*, 1705942.
[7] S. K. Kihoi, J. N. Kahiu, H. Kim, U. S. Shenoy, D. K. Bhat, S. Yi, H. S. Lee, *J. Mater. Sci. Technol.* **2021**, *85*, 76.
[8] S. Chen, Z. Ren, *Mater. Today* **2013**, *16*, 387.
[9] C. Fu, Y. Liu, X. Zhao, T. Zhu, *Adv. Electron. Mater.* **2016**, *2*, 1600394.
[10] K. S. Kim, Y. M. Kim, H. Mun, J. Kim, J. Park, A. Y. Borisevich, K. H. Lee, S. W. Kim, *Adv. Mater.* **2017**, *29*, 1702091.
[11] Y. Wu, Z. Chen, P. Nan, F. Xiong, S. Lin, X. Zhang, Y. Chen, L. Chen, B. Ge, Y. Pei, *Joule* **2019**, *3*, 1276.
[12] S. il Kim, K. H. Lee, H. A. Mun, H. S. Kim, S. W. Hwang, J. W. Roh, D. J. Yang, W. H. Shin, X. S. Li, Y. H. Lee, G. J. Snyder, S. W. Kim, *Science* **1979**, *2015*, 348.
[13] B. Poudel, Q. Hao, Y. Ma, Y. Lan, A. Minnich, B. Yu, X. Yan, D. Wang, A. Muto, D. Vashaee, X. Chen, J. Liu, M. S. Dresselhaus, G. Chen, Z. Ren, *Science* **2008**, *320*, 634.
[14] X. Zhang, D. Wang, H. Wu, M. Yin, Y. Pei, S. Gong, L. Huang, S. J. Pennycook, J. He, L. D. Zhao, *Energy Environ. Sci.* **2017**, *10*, 2420.
[15] M. R. Burton, S. Mehraban, D. Beynon, J. McGettrick, T. Watson, N. P. Lavery, M. J. Carnie, *Adv. Energy Mater.* **2019**, *9*, 1900201.
[16] M. R. Burton, T. Liu, J. McGettrick, S. Mehraban, J. Baker, A. Pockett, T. Watson, O. Fenwick, M. J. Carnie, *Adv. Mater.* **2018**, *30*, 1801357.
[17] J. P. Heremans, V. Jovovic, E. S. Toberer, A. Saramat, K. Kurosaki, A. Charoenphakdee, S. Yamanaka, G. J. Snyder, *Science* **2008**, *321*, 554.

[18] Y. Wu, P. Nan, Z. Chen, Z. Zeng, R. Liu, H. Dong, L. Xie, Y. Xiao, Z. Chen, H. Gu, W. Li, Y. Chen, B. Ge, Y. Pei, *Adv. Sci.* **2020**, *7*, 1902628.
[19] I. T. Witting, T. C. Chasapis, F. Ricci, M. Peters, N. A. Heinz, G. Hautier, G. J. Snyder, *Adv. Electron. Mater.* **2019**, *5*, 1800904.
[20] B. Russ, A. Glaudell, J. J. Urban, M. L. Chabinyc, R. A. Segalman, *Nat. Rev. Mater.* **2016**, *1*, 16050.
[21] Y. Zhang, W. Wang, F. Zhang, K. Dai, C. Li, Y. Fan, G. Chen, Q. Zheng, *Small* **2022**, *18*, 2104922.
[22] W. Ma, K. Shi, Y. Wu, Z. Y. Lu, H. Y. Liu, J. Y. Wang, J. Pei, *ACS Appl. Mater. Interfaces* **2016**, *8*, 24737.
[23] L. Wang, B. Dong, R. Ge, F. Jiang, J. Xu, *ACS Appl. Mater. Interfaces* **2017**, *9*, 7108.
[24] D. Huang, C. Wang, Y. Zou, X. Shen, Y. Zang, H. Shen, X. Gao, Y. Yi, W. Xu, C. Di, D. Zhu, *Angew. Chem.* **2016**, *128*, 10830.
[25] J. S. Yun, S. Choi, S. H. Im, *Carbon Energy* **2021**, *3*, 667.
[26] J. L. Blackburn, A. J. Ferguson, C. Cho, J. C. Grunlan, *Adv. Mater.* **2018**, *30*, 1704386.
[27] T. Juntunen, H. Jussila, M. Ruoho, S. Liu, G. Hu, T. Albrow-Owen, L. W. T. Ng, R. C. T. Howe, T. Hasan, Z. Sun, I. Tittonen, *Adv. Funct. Mater.* **2018**, *28*, 1800480.
[28] P. an Zong, J. Liang, P. Zhang, C. Wan, Y. Wang, K. Koumoto, *ACS Appl. Energy Mater.* **2020**, *3*, 2224.
[29] Z. Yan, D. L. Nika, A. A. Balandin, *IET Circuits, Devices Syst.* **2015**, *9*, 4.
[30] P. Dollfus, V. H. Nguyen, J. Saint-Martin, *J. Phys. Condens. Matter* **2015**, *27*, 133204.
[31] E. Pop, V. Varshney, A. K. Roy, *MRS Bull.* **2012**, *37*, 1273.
[32] Q. Y. Li, T. Feng, W. Okita, Y. Komori, H. Suzuki, T. Kato, T. Kaneko, T. Ikuta, X. Ruan, K. Takahashi, *ACS Nano* **2019**, *13*, 9182.
[33] S. Rafique, M. R. Burton, N. Badiei, J. E. Gonzalez-Feijoo, S. Mehraban, M. Carnie, A. Tarat, L. Li, *ACS Appl. Mater. Interfaces* **2020**, *12*, 30643.
[34] P. Thiyagarajan, M. W. Oh, J. C. Yoon, J.-H. Jang, *Appl. Phys. Lett.* **2014**, *105*, 033905.
[35] L. Qiu, P. Guo, H. Zou, Y. Feng, X. Zhang, S. Pervaiz, D. Wen, *ES Energy Environ.* **2018**, *2*, 66.
[36] K. J. Peng, C. L. Wu, Y. H. Lin, Y. J. Liu, D. P. Tsai, Y. H. Pai, G. R. Lin, *J. Mater. Chem. C* **2013**, *1*, 3862.
[37] M. Gautam, Z. Shi, A. H. Jayatissa, *Sol. Energy Mater. Sol. Cells* **2017**, *163*, 1.
[38] T. J. Slade, S. Anand, M. Wood, J. P. Male, K. Imasato, D. Cheikh, M. M. al Malki, M. T. Agne, K. J. Griffith, S. K. Bux, C. Wolverton, M. G. Kanatzidis, G. J. Snyder, *Joule* **2021**, *5*, 1168.
[39] G. J. Snyder, E. S. Toberer, *Nat. Mater.* **2008**, *7*, 105.
[40] S. Chen, Q. Wu, C. Mishra, J. Kang, H. Zhang, K. Cho, W. Cai, A. A. Balandin, R. S. Ruoff, *Nat. Mater.* **2012**, *11*, 203.
[41] A. A. Balandin, S. Ghosh, W. Bao, I. Calizo, D. Teweldebrhan, F. Miao, C. N. Lau, *Nano Lett.* **2008**, *8*, 902.
[42] S. Ghosh, D. L. Nika, E. P. Pokatilov, A. A. Balandin, *New J. Phys.* **2009**, *11*, 095012.
[43] S. Chen, A. L. Moore, W. Cai, J. W. Suk, J. An, C. Mishra, C. Amos, C. W. Magnuson, J. Kang, L. Shi, R. S. Ruoff, *ACS Nano* **2011**, *5*, 321.
[44] S. Ghosh, W. Bao, D. L. Nika, S. Subrina, E. P. Pokatilov, C. N. Lau, A. A. Balandin, *Nat. Mater.* **2010**, *9*, 555.
[45] J. H. Seol, I. Jo, A. L. Moore, L. Lindsay, Z. H. Aitken, M. T. Pettes, X. Li, Z. Yao, R. Huang, D. Broido, N. Mingo, R. S. Ruoff, L. Shi, *Science* **2010**, *328*, 213.
[46] R. Murali, Y. Yang, K. Brenner, T. Beck, J. D. Meindl, *Appl. Phys. Lett.* **2009**, *94*, 243114.
[47] Y. Anno, Y. Imakita, K. Takei, S. Akita, T. Arie, *2D Mater.* **2017**, *4*, 025019.
[48] M. Uzair Khan, A. Naveed, S. Ehtisham Gillani, D. Awan, M. Arif, S. Afridi, M. Hamyun, M. Asif, S. Tabassum, M. Sadiq, M. Lais, M. Aslam, S. Ullah Jan, Z. Ahad, *Mater. Res. Express* **2021**, *8*, 056302.
[49] H. Xie, *J. Mater. Sci.* **2007**, *42*, 3695.
[50] P. E. Khizhnyak, A. V. Chechetkin, A. P. Glybin, *J. Eng. Phys.* **1979**, *37*, 1073.
[51] R. Prasher, *Science* **2010**, *328*, 185.
[52] N. K. Mahanta, A. R. Abramson, in *13th InterSociety Conference on Thermal and Thermomechanical Phenomena in Electronic Systems*, IEEE, **2012**, pp. 1–6.